Monitoring Solar Flare-Induced SIDs with Radio Science Instrumentation

Kimberly Coates

PH 499 / HON 499

Advisors: Dr. Nazirah Jetha & Dr. Linda Krause

Background: Space Weather and the Ionosphere

Space weather is "the study of how variations in the space environment near the Earth affect technological systems and humans" (Hapgood and Cargill 2000, 2.31-2.32). Currently, space weather is an extremely important topic because of the amount of technology affected by it. Satellites, spacecraft, and even Earth-based devices are subject to the hazards of the space weather environment caused by transient, energetic disturbances (Bushell 2008, 244-245). Space weather affects the way radio waves propagate through the ionosphere, which can in turn affect the operation of GPS systems on Earth. Sudden ionospheric disturbances caused by solar flares can interfere with communications technology, and solar flares can also be hazardous to some satellites. A build up of charged particles from solar flares can cause circuits to become overloaded with current, destroying sensitive electrical components. Understanding sudden ionospheric disturbances, and thus solar flares, is the first step in preventing damage to these technologies.

Solar flares occur in magnetically active regions of the Sun. Active regions are rare during the solar minimum of the Sun's 11-year cycle, but during solar maximum, their frequency of occurrence increases significantly (Holmon and Benedict 2007). As such, solar flares are more common during times of solar maximum. During a solar flare, energy is released from the sun in the form of plasma, electromagnetic radiation (particularly in the ultraviolet and x-ray portion of the spectrum), and, occasionally, energetic protons and electrons. Solar flares are assigned a class, B, C, M, or X, and a multiplier (which indicates the level of intensity within a class) according to their peak of intensity of x-ray output from wavelength .1 to .8 nm as measured from the Earth (Lee

2008). For instance, a B6.5 class flare is smaller than a C1.3 class flare, and an X1.5 class flare is larger than both the B6.5 and the C1.3 flare.

The ionosphere is a layer of cold, magnetized plasma in the Earth's upper atmosphere, roughly 70 km to 1000 km from the Earth's surface. Radiation from the Sun interacts with the upper atmosphere in such a way as to create the stratified F, E, and D-regions of the ionosphere, as depicted in Figure 1 (Bushell 2008, 244-245). Emissions from solar flares increase the ionization level of the lower layers of the ionosphere on the daytime side of the Earth (Cohen and Davies 1994). These emissions excite particles in the atmosphere, releasing electrons through the mechanism of photo-ionization. These excited electrons then
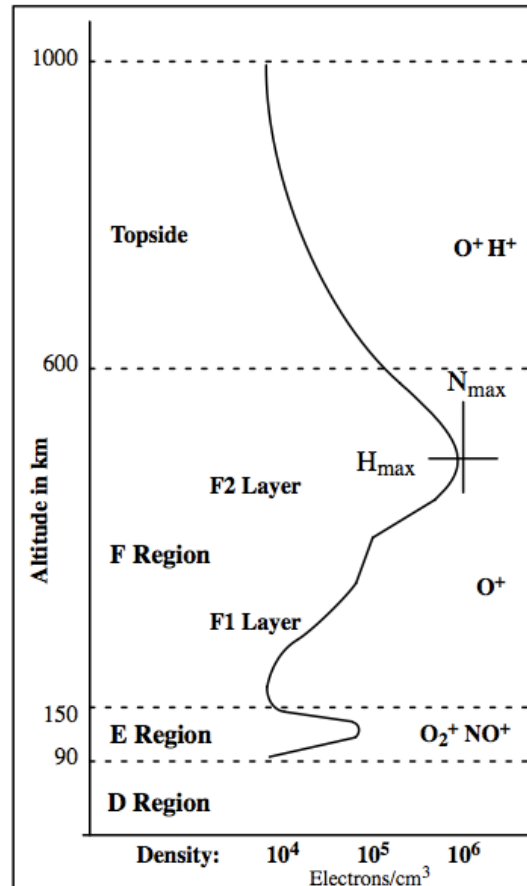

Figure 1: The Ionosphere
From: Anderson, Dave and Tim Fuller-Rowell. "The Ionosphere." (1999).

excite other electrons in a trickle-down effect known as electron precipitation. This event of an increase in ionization in the ionosphere is known as a sudden ionospheric disturbance (SID). This increase in ionization results in an increased electron density on the day time side of Earth. Put another way, an SID is an area of high plasma density in the ionosphere (Petruzzellis 2008, 153-164). Ionization levels also affect a parameter known as total electron content, or TEC, which is a measure of electrons per square meter that indicates the delay of a radio signal along a given path (Anderson and Fuller-

Rowell 1999).

Electron density affects how radio waves propagate along the waveguide in between the Earth's ionosphere and the ground (Scherrer et al. 2009). High frequency (HF) radio waves are absorbed in areas of high electron concentration in a process known as Short Wave Fadeout, where as very low frequency waves (VLF, roughly 10^4 Hz) propagate more efficiently in areas of higher electron density (Petruzzellis 2008, 153-164). This is due to how VLF waves propagate along the waveguide. In general, the waves are being reflected from the lower layers of the ionosphere, and when the ionosphere has a higher electron density, there are more electrons for the waves to reflect off of, thereby increasing the signal intensity of the radio waves. Conversely, if the electron density is low, the signal strength is lower due to the signal intensity deteriorating as it loses energy while it penetrates into deeper layers of the ionosphere rather than being reflected. During the day, radiation from the Sun causes the ionosphere to separate into layers that vary according to electron density. The bottom layer, the D layer, is generally not very dense. Consequentially, radio waves pass through it to the next layer, the E layer, where they are reflected back down through the D layer to the ground (Stanford 2009). During this process, the signal loses energy passing through the D layer, thus weakening the signal strength as it travels. However, in the event of a solar flare, the D layer becomes temporarily ionized due to the stream of charged particles from the solar flare hitting the atmosphere. When the D layer is ionized in this way, VLF signals can bounce off of the D layer instead of the E layer, making the distance of reflection shorter and preserving the integrity of the signal strength. As such, VLF waves, because of how they interact with the ionosphere during

SIDs, can be used to detect SIDs, and, consequentially, solar flares. As shown in Figure 2, VLF stations transmit VLF radio waves into the ionosphere, where they interact with the ionospheric environment. These VLF signals are then received by an SID monitor, and ionospheric characteristics can be determined from how the waveforms have been modulated during their travel from transmission to reception. The intensity of the VLF signals are tracked over time. Solar flares are distinguished from other SIDs shown in the data by the characteristically abrupt spike and subsequent oblique decline in intensity that they exhibit.
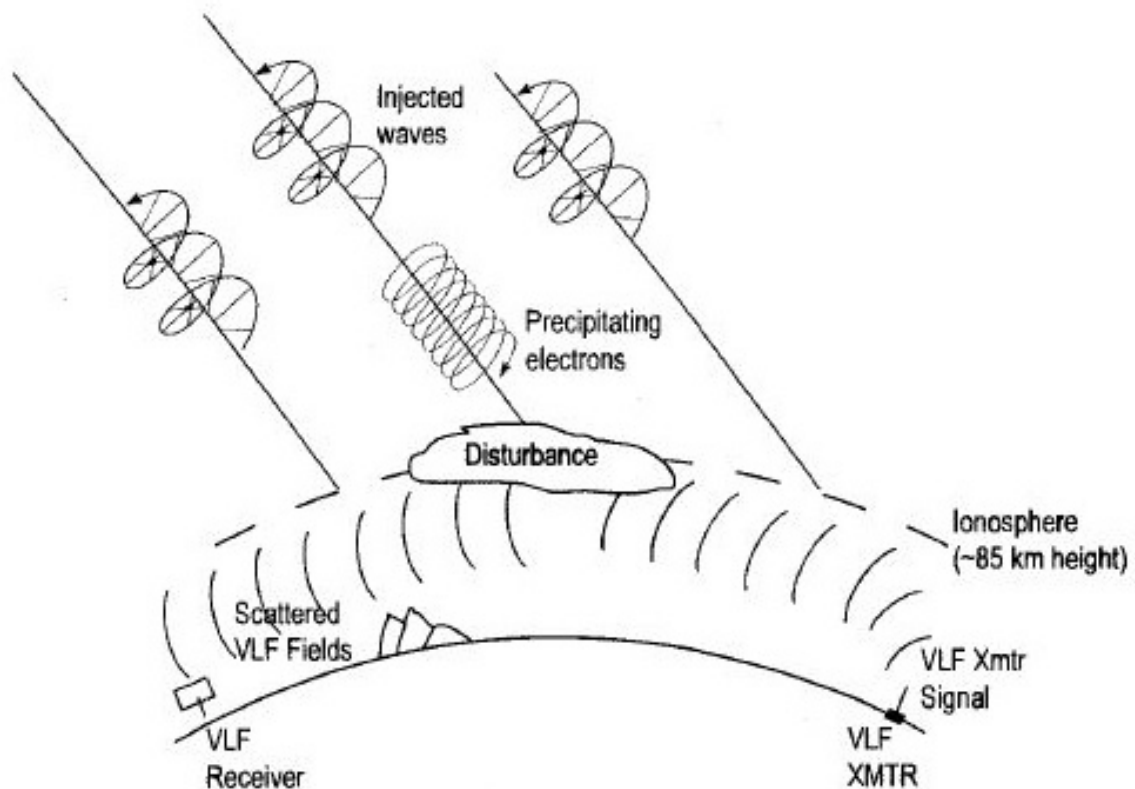

Figure 2: Using VLF Waves to Detect SIDs
Image Courtesy of HAARP

Instrumentation

The design for a SID monitor involves an induction-loop antenna to receive the transmitted VLF signal and a SID receiver to amplify and record the signal. In general, SID receivers incorporate the use of operational amplifiers to amplify the signal strength of the received VLF signal, and potentiometers to create a low-pass filter to eliminate high-frequency signal noise. This allows the receiver to focus in on the VLF signal being received from the VLF transmitter and record a cleaner signal for more accurate data.

In an effort to better understand circuit theory, construction, and troubleshooting in preparation for understanding how the circuits utilized in SID detectors operate, two types of circuits were constructed utilizing 555 timer astable multivibrator chips. The 555 timer astable multivibrator is a chip commonly used to make oscillations or time delays, in this case for the purpose of pulse generation. The circuits were then tested using an oscilloscope to monitor the output waveforms. Lastly, for the circuit analysis portion of the project, operational amplifiers were studied as they are used in the amplification of the input signal of SID receivers.

The first circuit was a simple oscillating circuit constructed using the LM 555 timer, 1µF and .1µF capacitors, and assorted resistors with its output shown as a blinking LED (shown in Figures 3 and 4).
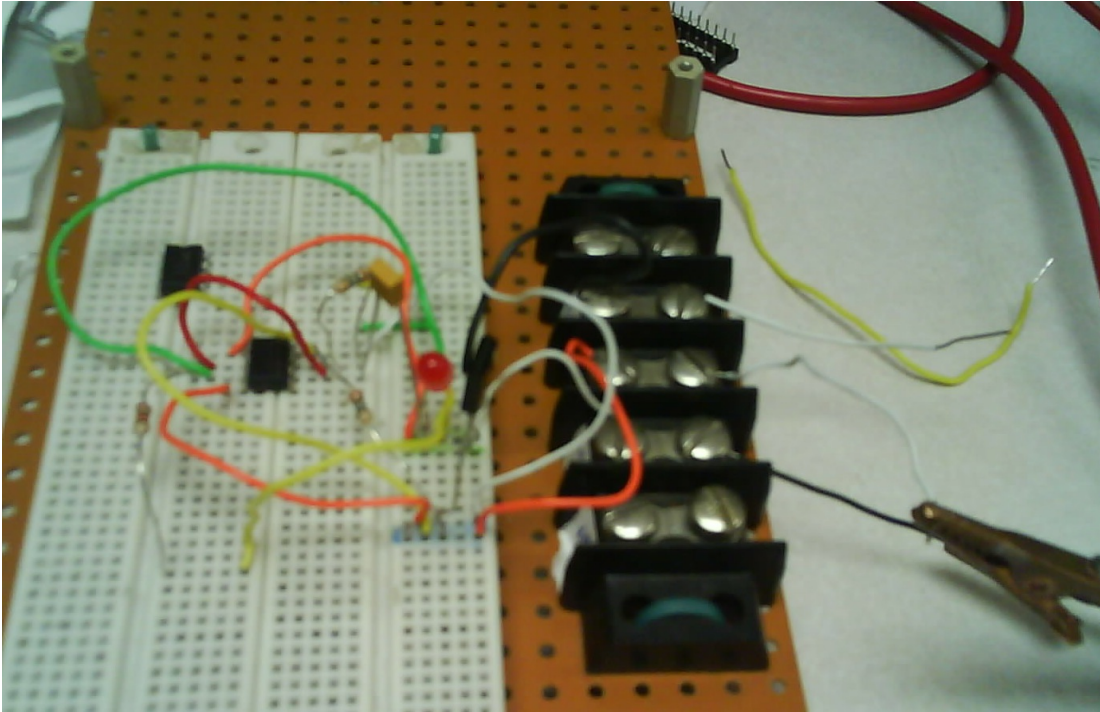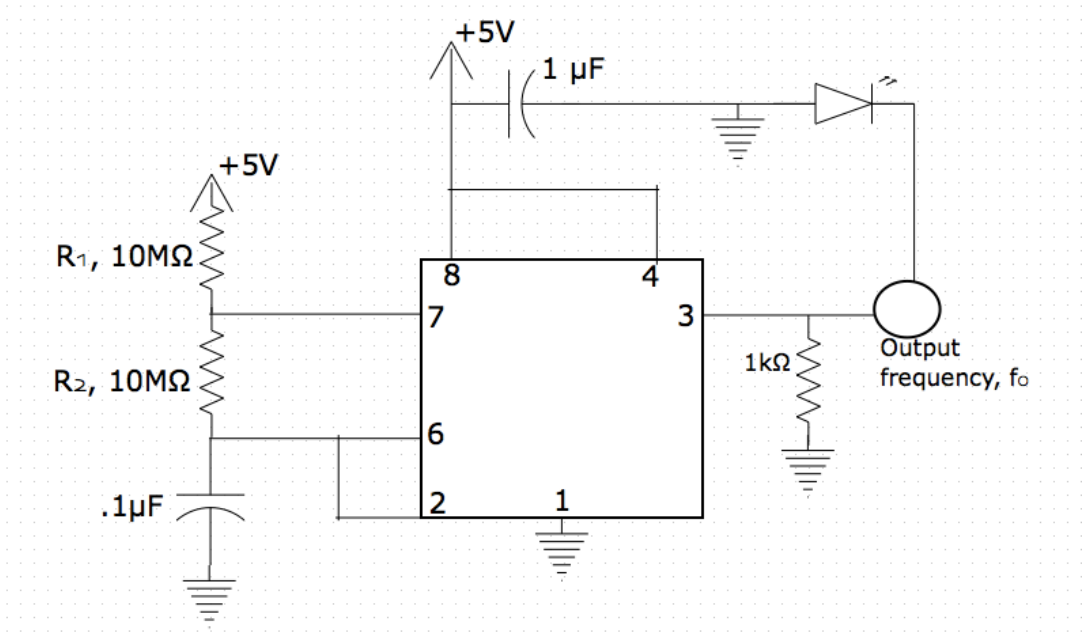
Figure 3: Simple Oscillating Circuit

Figure 4: Simple Oscillating Circuit Diagram (Constructed using Diagramly, www. diagram.ly)

The equation for output frequency

$$f_o=1.44/[(R_1+2R_2)C]$$

was used to understand how adding more resistance changes the output frequency.

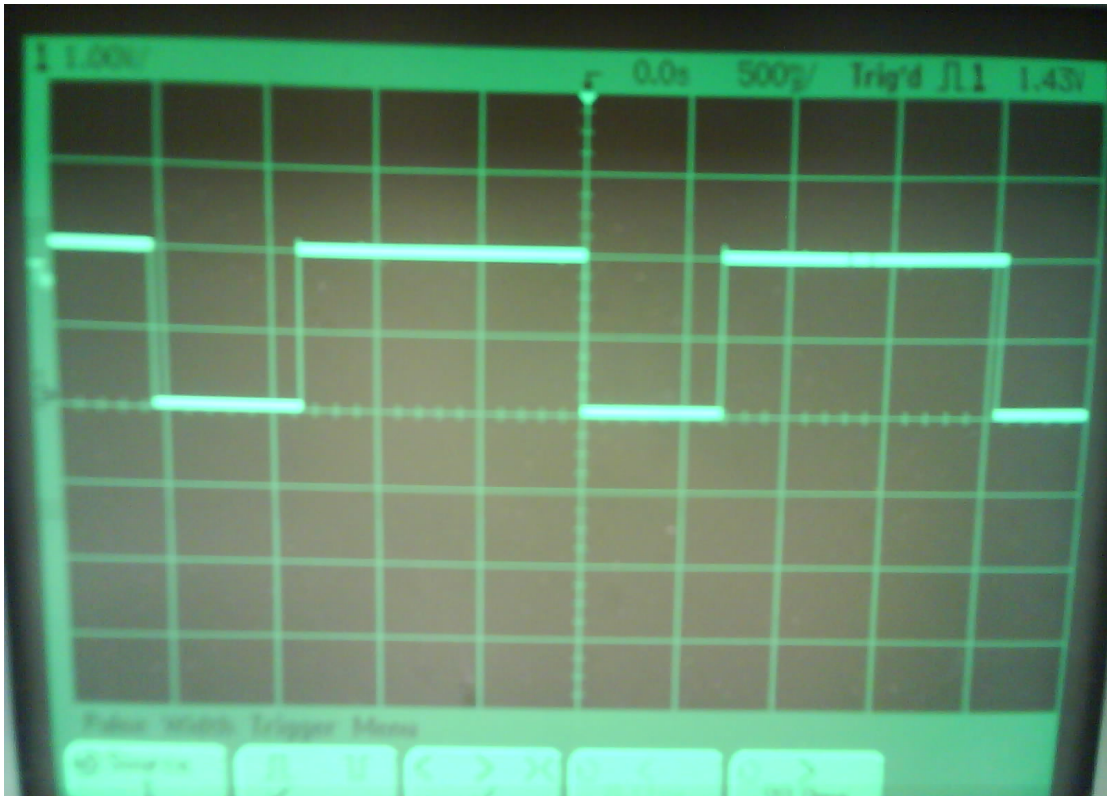A sample output for the oscillating circuit is shown below.

Figure 5: Output for a Simple Oscillating Circuit

The percent duty cycle

$$\%D = [(R_1 + R_2) / (R_1 + 2R_2)] \times 100\%$$

was then examined by varying R_2, the result of which is shown in Figures 6 and 7.
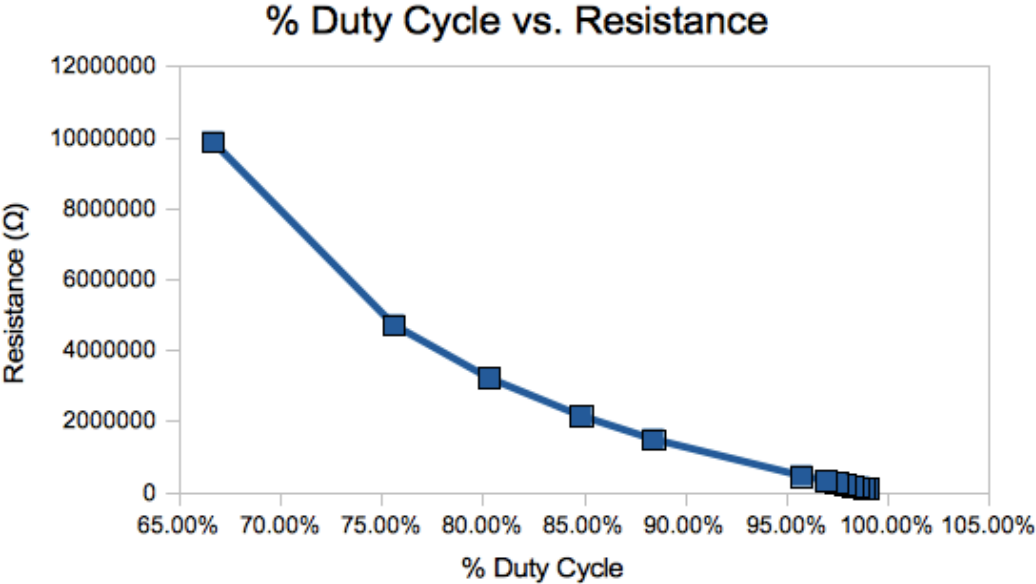
% Duty Cycle vs. Resistance

Figure 6 (above): Graph of % Duty Cycle vs. Resistance.
Figure 7 (below): Table of Values of Resistance and Duty Cycle over Time

R1 (Ω)	R2 (Ω)	time (s)	duty cycle
9.88E+06	9.90E+04	3.16E-02	99.02%
9.88E+06	1.18E+05	4.00E-02	98.83%
9.88E+06	1.47E+05	5.00E-02	98.55%
9.88E+06	1.77E+05	6.00E-02	98.27%
9.88E+06	2.17E+05	7.40E-02	97.89%
9.88E+06	2.66E+05	9.00E-02	97.44%
9.88E+06	3.24E+05	1.10E-01	96.92%
9.88E+06	4.63E+05	1.59E-01	95.72%
9.88E+06	1.49E+06	5.10E-01	88.41%
9.88E+06	2.15E+06	7.90E-01	84.84%
9.88E+06	3.21E+06	1.10E+00	80.31%
9.88E+06	4.71E+06	1.63E+00	75.60%
9.88E+06	9.87E+06	3.40E+00	66.68%

As expected, the results show that with an increase in R_2, there is a decrease in the

percent duty cycle (i.e. the LED blinks on longer when more resistance is applied).

The next circuit was constructed using two LM 555 timer chips, one .01 μF

capacitor, and one 9.87 kΩ resistor to create a pulse width modulator (Figures 8 and 9).
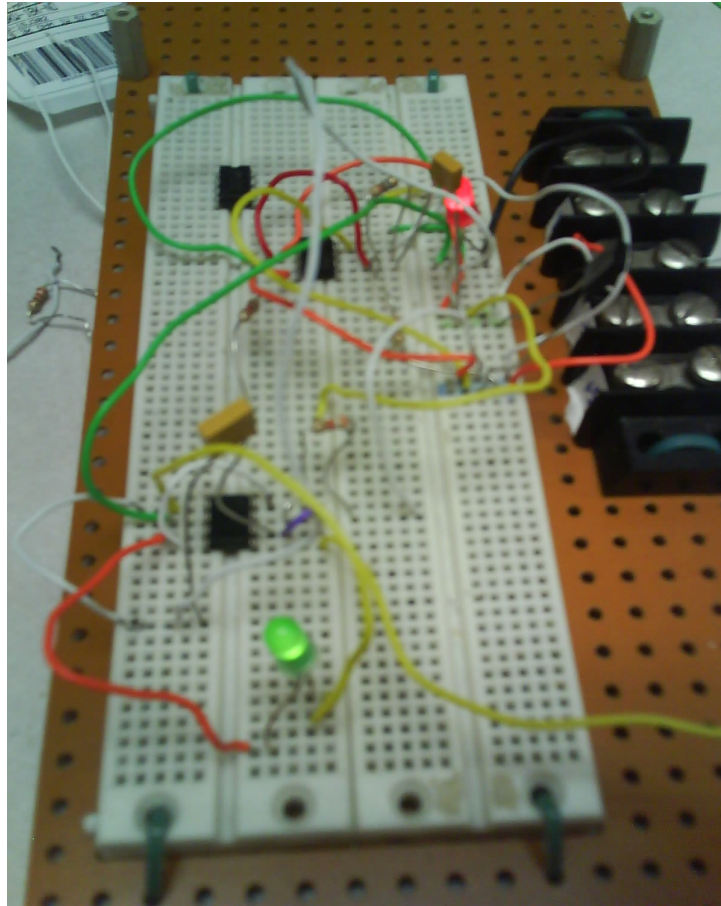
Figure 8: Pulse Width Modulating Circuit

The green LED shows how the output varies from the modulation input. Increasing the

input current increased the brightness output of the LED, and decreasing the input

current decreased the brightness output of the LED, effectively working like a dimmer

switch. Unfortunately, the oscilloscope was ineffective at the low frequency being used

with the pulse width modulation circuit, so data collected at this step was, for the most
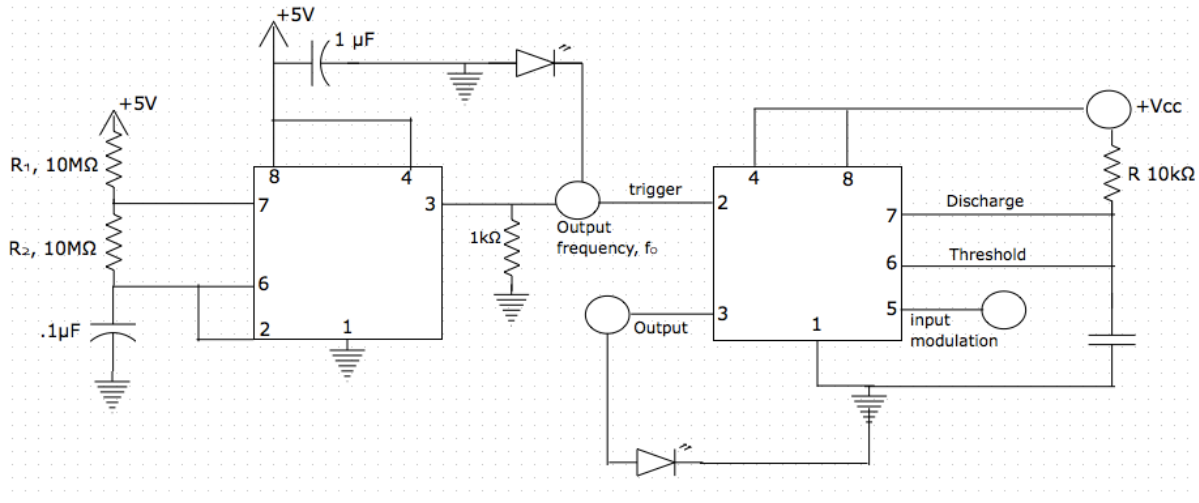
part, unreliable.

Figure 9: Pulse Width Modulating Circuit Diagram (Constructed using Diagramly, www. diagram.ly)

Data Analysis

For this project, data from Stanford's SOLAR Center and NOAA's Space Weather Prediction Center was studied. SID monitors collect data from multiple VLF transmitting stations simultaneously, and this data is then uploaded to these online databases. This data is interpreted as VLF signal intensity over time. Most SID monitors can only detect solar flares of class C1.0 or larger, however, very intense X-class flares exceed the capabilities of SID monitors and cause them to record data that peaks off charts (Lee 2008).

In SID data, sunrise generally exhibits a steep and sudden drop from a higher signal strength to a relatively lower signal strength. Alternatively, sunset exhibits a steep and sudden increase in signal strength. Because signal strength is increased for all disturbances, solar flare-induced SID signatures can be lost amongst the rest of the signals. For this reason, data that occurs before 1200 to 1400 (UT) is generally ignored because it is in the night time (Lee 2008). This phenomenon of signal strength

increasing during the night time is due to the reflective properties of the ionosphere, quantified by a characteristic called the reflection coefficient, which is dependent upon the frequency of the radio signal being used and the electron density of the given region of the ionosphere under consideration at the time (Petruzzellis 2008, 153-164). At night, the distance is longer between where the signal reflects from the ground on Earth to the ionosphere than it is during the daytime. The electron density during the day time ranges from 10 electrons/cm³ to 10,000 electrons/cm³ as altitude is increased from 40 km to 85 km, where as at night it only ranges from 10 electrons/cm³ to 1000 electrons/cm³ from 85 km to 140 km, with the lower D-region essentially becoming nonexistent (Petruzzellis 2008, 153-164). Another phenomenon that affects the signal strength of SID data throughout the period of a day is the "normal quiescent daytime pattern," which refers to the VLF signal strength increase, peak, and decline that occurs corresponding to sunrise, noon, and sunset (Beck 2011).

During the course of this project, the Sun has been entering a period of solar maximum in its 11-year cycle. Fortunately, this means there was plenty of recent SID data from solar flares to study and compare. Figure 10 shows information collected by the U.S. Department of Commerce, NOAA, and the Space Weather Prediction Center (SWPC) for SIDs that occurred on March 17th, 2012.

#Event	Begin	Max	End	Type	Particulars
3360+	300	312	318	XRA	C1.0
3370	833	1120	1159	XRA	B3.8
3500	A1558		A0935	DSF	9
3380+	1617		1618	RSP	III/1
3400	1804	1814	1825	XRA	B6.0
3410	2032	2039	2042	XRA	M1.3
3410+	2035		2043	RSP	III/2
3410	2036	2039	2053	FLA	SF
3410+	2036	2036	2036	RBR	110
3410+	2036	2036	2037	RBR	160
3410+	2036	2038	2038	RBR	610
3410	2036	2036	2036	RBR	54
3410	2037	2037	2037	RBR	67
3410+	2038		2045	RSP	II/2
3420	2320	2341	2355	XRA	B8.1

Figure 10: SID Data: Solar Flare Event of March 17, 2012

The column "#Event" gives the event number, "Begin" gives the start time of a given

event (in UT), "Max" gives the time that the event peaked in intensity, "End" gives the

end time of the event, "Type" indicates the kind of event, and "Particulars" indicates the

classification of the given event (Lee 2008). Solar flares are classified as "XRA" under

type, indicating that on March 17, 2012 there were five solar flares of varying intensities

from B3.8 to M1.3. Particularly of interest is the confirmed solar flare of class M1.3

(shown in red), for which corresponding data from the Stanford SOLAR center database

was found. Using the data from SOLAR, a graph of intensity over time was made in

Excel (Figure 11). A distinct spike in intensity can be seen around the time of 9:00 PM

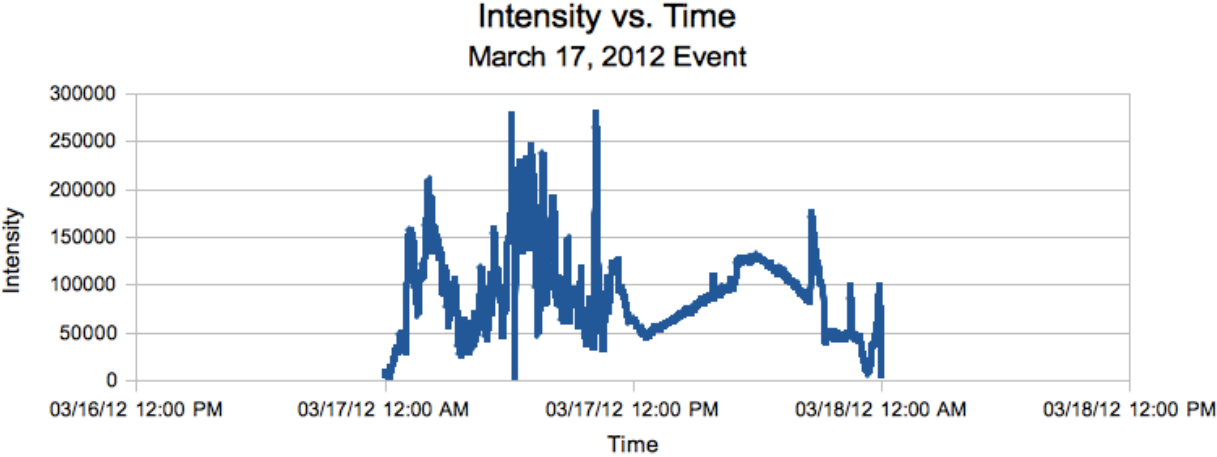March 17, 2012. This is the solar flare identified in the NOAA data.

Figure 11: SID Data: Solar Flare Event of March 17, 2012

This spike shows that there is a distinct relationship between VLF signal intensity and solar flare-induced SIDs. Figure 12, the intensity verse time graph from the SOLAR database website, shows this spike more clearly (black arrows indicate the times of sunrise and sunset). It is comprised of data from the monitor site, BRASSO, which detected the M1.3 solar flare at ~20:30 UT.
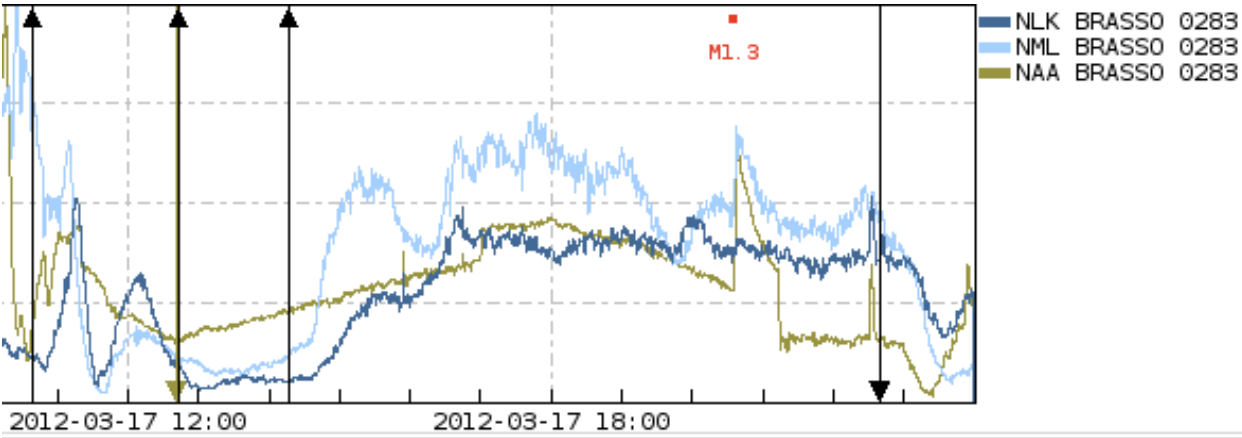

Figure 12: SID Data: Solar Flare Event of March 17, 2012
From: Stanford SOLAR Center

Some monitors in the SOLAR database showed data that had no clear day time/ night time intensity variation, while others did not show SIDs from documented and

verified solar flare events. Also, some monitors showed no data at all for given periods

of time. Figure 13, below, shows data from a particular monitor site, WB9RIM, which did

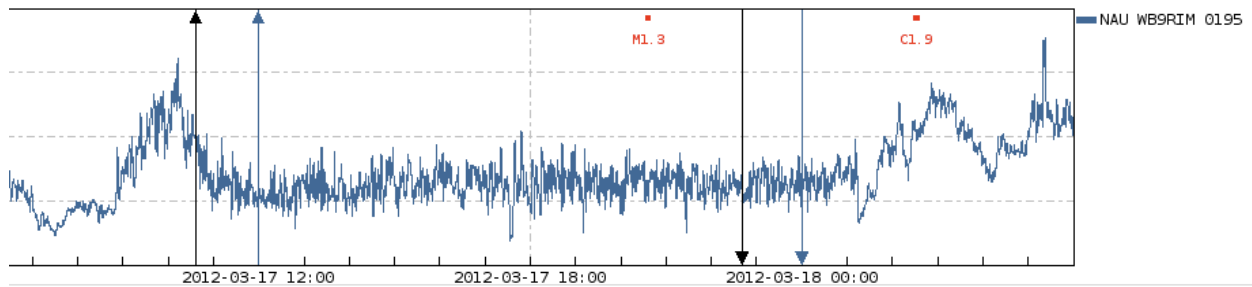not pick up the March 17, 2012 M1.3 solar flare.

Figure 13: Unreliable SID Data
From: Stanford SOLAR Center

After contacting William Lord from the Stanford SOLAR Center, these inconsistencies

with SID data from various monitors were addressed. Some SID data sets submitted

from large cities are inconsistent with respect to day time/night time intensity variation

due to interference from the higher radio-frequency noise levels present in the

environment. On top of this, some monitors are not collecting reliable data because they

have not been properly configured. Aside from instrumentation issues, there are several

physical explanations for SID data inconsistency. For instance, it is possible that some

of the inconsistent SID data is due to ionospheric scintillation, which affects how radio

waves travel through the ionosphere, particularly if the data came from stations at high

latitude, where the ionosphere is susceptible during the daytime or the nighttime to this

condition. Ionospheric scintillation is caused by turbulence due to small-scale

irregularities in plasma density (Anderson and Fuller-Rowell 1999). Solar flares can

actually result in a decrease in signal strength instead of the desired increase in signal

strength (Stanford 2009). This occurs because, during a solar flare, VLF waves reflect

at lower altitudes because lower layers of the ionosphere become more ionized. At these lower altitudes, the atmosphere tends to be thicker, thus leading to more collisions between particles and the radio waves. These collisions can result in destructive interference, which causes a decrease in signal strength of the solar flare-induced SIDs. Geomagnetic substorms and particle precipitation from the Earth's radiation belts can also affect the electron density of the ionosphere, thereby obscuring solar flare-induced SID data (Kavanagh et al. 2011).

Works Cited

Anderson, Dave and Tim Fuller-Rowell. "The Ionosphere." *Space Environment Topics*
    SE-14 (1999). Accessed April 3, 2012.
    http://www.swpc.noaa.gov/Education/index.html.

Beck, Sara J. "Sudden Ionospheric Disturbances (SIDs)." Last modified March 21, 2011.
    AAVSO. Accessed April 12, 2012. http://www.aavso.org/solar-sids.

Bushell, Andrew C. "Space weather: from mud to magnetopause." *Weather* 63, no. 8
    (2008): 244-245.

Cohen, Norm and Kenneth Davies. "Radio Wave Propagation." *Space Environment
    Topics* SE-10 (1994). Accessed April 3, 2012.
    http://www.swpc.noaa.gov/Education/index.html.

Everding, Daniel. "SIMONE: Building an SID Detector for Space Weather Monitoring."
    Bachelor's thesis, University of Alabama in Huntsville, 2011.

Hapgood, Mike and Peter Cargill. "Space Weather." *A&G* 41, (2000): 2.31-2.32.

Holman, Gordon and Sarah Benedict. "What is a Solar Flare?" Last modified August 1,
    2007. NASA Goddard Space Flight Center. Accessed April 12, 2012.
    http://hesperia.gsfc.nasa.gov/sftheory/flare.htm.

Kavanagh, A. J. et al. "Probing geospace with VLF radio signals." *A&G* 52, (2011):
    2.27-2.30.

Lee, Shannon. "Getting Started With SID Data." Last modified 2008. Stanford SOLAR
    Center. Accessed April 7, 2012.
    http://solar-center.stanford.edu/SID/data/data-access.html.

Petruzzellis, Thomas. "VLF or Very Low Frequency Radio Receiver." in *22 Radio and
    Receiver Projects for the Evil Genius,* 153-164. New York: McGraw-Hill, 2008.

Scherrer, Deborah et al. "Super SID Manual: Space Weather Monitors." *Stanford
    University SOLAR Center,* (2009).

Stanford SOLAR Center. 2009. "Tracking Solar Flares." Accessed April 23, 2012.
    http://solar-center.stanford.edu/SID/activities/ionosphere.html.